Acta Oceanol. Sin., 2023, Vol. 42, No. 3, P. 19–30
https://doi.org/10.1007/s13131-022-2078-1
http://www.aosocean.com
E-mail: ocean2@hyxb.org.cn

Zircon U-Pb geochronology, Hf isotopes, and geochemistry constraints on the age and tectonic affinity of the basement granitoids from the Qiongdongnan Basin, northern South China Sea

Lijun Mi[1†], Xiaoyin Tang[2, 3, 4*†], Haizhang Yang[1], Shuchun Yang[1], Shuai Guo[1]

[1] China National Offshore Oil Corporation (CNOOC) Research Center, Beijing 100028, China

[2] Institute of Geomechanics, Chinese Academy of Geological Sciences, Beijing 100081, China

[3] Key Laboratory of Paleomagnetism and Tectonic Reconstruction, Ministry of Natural Resources, Beijing 100081, China

[4] Key Laboratory of Petroleum Geomechanics, China Geological Survey, Beijing 100081, China

Received 1 March 2022; accepted 17 July 2022

Abstract

Studies in the northern South China Sea (SCS) basement remain important for understanding the evolution of the Southeast Asian continental margin. Due to a thick cover of sediments and scarce borehole penetration, little is known about the age and tectonic affinity of this basement. In this study, an integrated study of zircon U-Pb geochronology, Hf isotopes, and whole-rock major and trace elements on seven basement granitoids from seven boreholes of Qiongdongnan Basin has been carried out. New zircon U-Pb results for these granitoids present middle-late Permian ((270.0±1.2) Ma; (253±3.4) Ma), middle to late Triassic ((246.2±3.4) Ma; (239.3±0.96) Ma; (237.9±0.99) Ma; (228.9±1.0) Ma) and Late Cretaceous ages ((120.6±0.6) Ma). New data from this study, in combination with the previous dataset, indicates that granitoid ages in northern SCS basement vary from 270 Ma to 70.5 Ma, with three age groups of 270–196 Ma, 162–142 Ma, and 137–71 Ma, respectively. Except for the late Paleozoic-Mesozoic rocks in the basement of the northern SCS, a few old zircon grains with the age of (2 708.1± 17) Ma to (2 166.6±19) Ma provide clues to the existence of the pre-Proterozoic components. The geochemical signatures indicate that the middle Permian-early Cretaceous granitoids from the Qiongdongnan Basin are I-type granites formed in a volcanic arc environment, which were probably related to the subduction of the Paleo-Pacific Plate.

Key words: Qiongdongnan Basin, basement granitoids, geochemistry, U-Pb and Hf isotopes, Paleo-Pacific Plate subduction

Citation: Mi Lijun, Tang Xiaoyin, Yang Haizhang, Yang Shuchun, Guo Shuai. 2023. Zircon U-Pb geochronology, Hf isotopes, and geochemistry constraints on the age and tectonic affinity of the basement granitoids from the Qiongdongnan Basin, northern South China Sea. Acta Oceanologica Sinica, 42(3): 19–30, doi: 10.1007/s13131-022-2078-1

1 Introduction

The South China Sea (SCS) is one of the biggest marginal seas in the western Pacific region. Affected by the India-Eurasia collision to the northwest (Morley, 2002), the subduction of the Pacific Plate and then the compression from the Philippine Sea plate in the east (Zhou et al., 2002), as well as the slab-pull of the proto-SCS in the south (Taylor and Hayes, 1983), the evolution of the SCS is a key element in understanding tectonics in Southeast Asian. Previous studies of SCS have mainly focused on its Cenozoic tectonic evolution and several competing models have been proposed to explain the rifting to spreading process (Taylor and Hayes, 1980; Tapponnier et al., 1986; Cullen et al., 2010; Barckhausen et al., 2014). To better understand the Cenozoic tectonic evolution of the SCS, studies must be underpinned by the pre-Cenozoic tectonic framework within the basement, which exerted significant influence on the following evolutionary events. Therefore, the SCS Basin basement study has been the focus of structural geology and regional geodynamic reconstruction (Braitenberg et al., 2006; Cui et al., 2021).

Since the beginning of the 1980s, a series of studies have been performed on the basement of the northern SCS (Su et al., 1995; Liu et al., 2004a, b; Wang et al., 2002). Due to the thick Cenozoic sedimentary blanket and scarce borehole penetration, only the northeastern SCS region (Zhujiang River Mouth Basin) was modestly dated (Qiu et al., 1996; Li et al., 1999a; Zhou et al., 2002; Xu et al., 2017) while the extensive basement on northern SCS remains roughly constrained by petrographic observation and geophysical data, which lacked high-precision dating analyses (Lu et al., 2011, 2015; Sun et al., 2014). The limited geochronological investigation has long been a hindrance to the SCS Basin basement interpretation.

In this study, we reported new zircon U-Pb age, Hf isotopic compositions, and whole-rock major and trace elements of basement granitoids from the Qiongdongnan Basin (QDNB) on the

Foundation item: The National Natural Science Foundation of China under contract No. 42072181.
*Corresponding author, E-mail: xytang2019@126.com
†Authors contributed equally to this work.

northwestern end of the northern margin of the SCS. Integrated with previous data, the present study not only offers a substantial input to the geochronological knowledge of the northern SCS basement but also provides insights into the tectonic setting and evolution of the northern SCS.

2 Geological setting

The areas of northern SCS, as shown in Fig. 1a, are generally considered a southward extension of the South China Block (SCB) (Hayes and Nissen, 2005; Xu et al., 2013; Lei et al., 2016). The SCB, a major continental block in Southeast Asia, comprises the Yangtze Block in the northwest and the Cathaysia Block in the southeast. Since the amalgamation of the Yangtze and Cathaysia blocks in the early Neoproterozoic (Zhao and Cawood, 1999; Wang et al., 2013), the SCB has undergone complex tectonic events. There were events related to the Neoproterozoic supercontinent Rodinia breakup, featuring widespread bimodal igneous rocks, and continental rifting (Li et al., 1999b; Li et al., 2005a); subsequently, an early Paleozoic orogenic event was recorded by the angular unconformity between post-Silurian strata and the strongly-deformed pre-Devonian sediments with widespread granitic intrusions (Ren, 1964; Li et al., 2010); furthermore, a late Paleozoic-early Mesozoic orogenic event which resulted in the transition from a stable carbonate platform to clastic facies, orogenic uplift, and the formation of a basin-and-range style magmatic province (Li, 1998; Zhou et al., 2006; Li and Li, 2007). Widespread Mesozoic igneous rocks have been identified in the SCB, which formed over three main intervals: the early

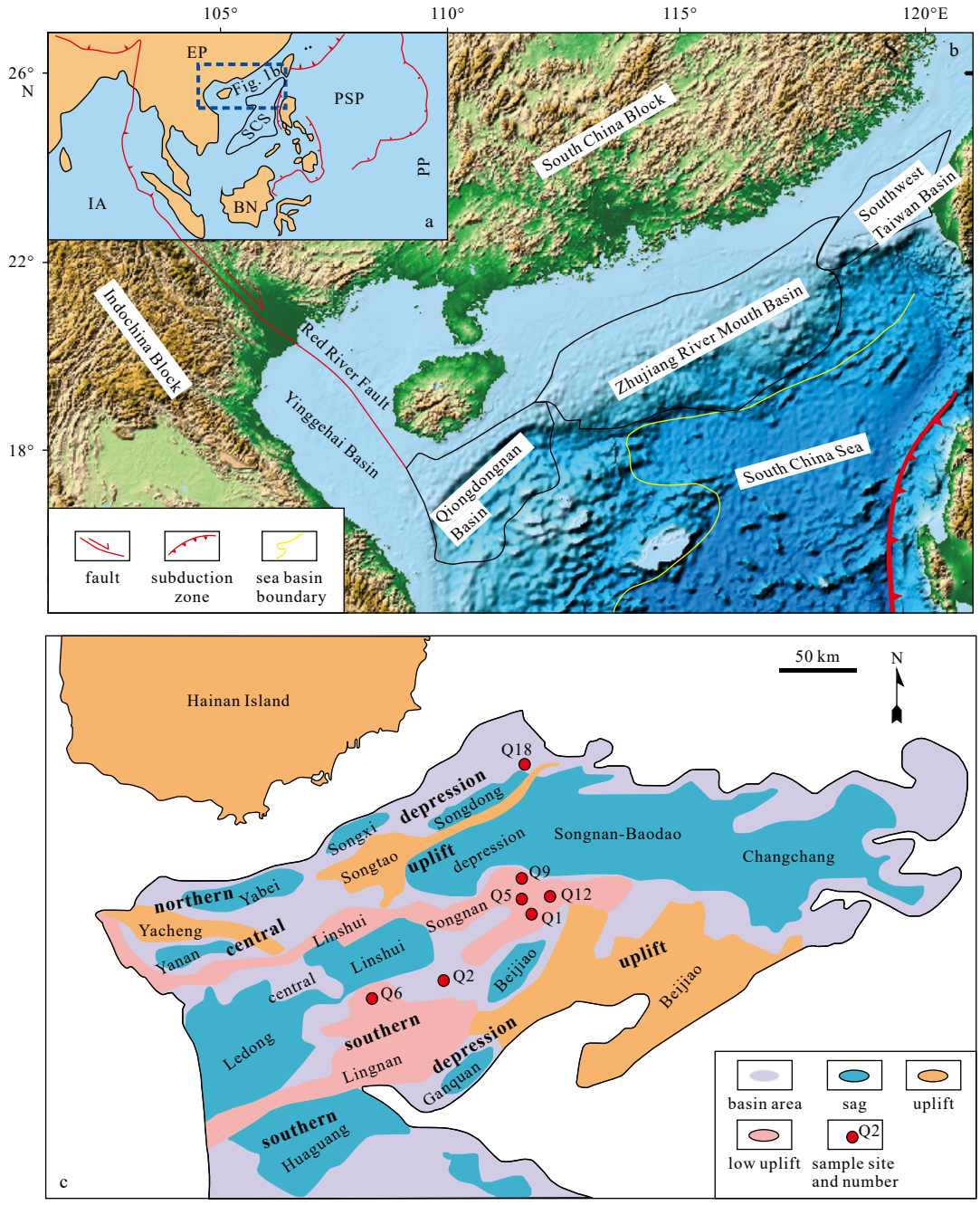

Fig. 1. Map showing the Qiongdongnan Basin in a regional context (a and b), and the basin tectonic units (c). Abbreviations in a: EP, Eurasian Plate; IA, India-Australian Plate; PSP, Philippine Sea Plate; SCS, South China Sea; PP, Pacific Plate; BN, Borneo.

Mesozoic or Indosinian (Triassic), the early Yanshanian (Jurassic), and the late Yanshanian (Cretaceous) (e.g., Zhou et al., 2006). It is generally accepted that these Mesozoic igneous rocks were related to the subduction of the Paleo-Pacific Plate, although it remains ambiguous how and when the Paleo-Pacific Plate subduction affected the continental margin of the SCB (Zhou and Li, 2000; Li and Li, 2007; Chen et al., 2008; Li et al., 2018).

The QDNB, overall NE trended, is located on the northwestern SCS margin. This basin is surrounded by the Hainan Island in the north, Yinggehai Basin in the west, Zhujiang River Mouth Basin in the east, and Xisha Block in the south (Fig. 1b). From north to the south, the QDNB consists of five first-order units: the Northern Depression, the Northern Uplift, the Central Depression, the Southern Uplift, and the Southern Depression (Liu et al., 2015; Meng et al., 2021). The Northern Depression could be further divided into the Yabei, Songxi, and Songdong sags from the west to the east, while the Central Depression consists of the Yanan, Ledong, Lingshui, Beijiao, Songnan-Baodao, and Changchang sags (Fig. 1c). The QDNB mainly underwent two structural evolution stages, i.e., the Eocene-Oligocene rifting stage and the Neogene-Quaternary post-rifting stage, and four tectonic events including the Shenhu, Zhujiang, Nanhai, and Dongsha movements (Zhu et al., 2009; Huang et al., 2016; Su et al., 2018). The filling sequences, from bottom to top, are Eocene, Yacheng formation (early Oligocene), Lingshui formation (late Oligocene), Sanya formation (early Miocene), Meishan formation (middle Miocene), Huangliu formation (late Miocene), Yinggehai formation (Pliocene), and Ledong formation (Quaternary), respectively (Cao et al., 2015; Su et al., 2018).

3 Sampling and methods

Seven basement granitoids from seven boreholes were collected from the core library of China National Offshore Oil Corporation (CNOOC) Co., Ltd., Shenzhen, China (locations see Fig. 1c). Zircon grains were separated using standard density and magnetic separation techniques at the Chengxin Geological Services Co. LTD, Langfang, China. Typically, more than 300 zircon grains from each sample were randomly adhered to adhesive tape and then cast in an epoxy mount before the polishing process. The analytical spots were chosen based on careful examination of transmitted and reflected light micrographs as well as cathodoluminescence (CL) images for internal morphology before analysis.

3.1 *U-Pb dating*

Zircon U-Pb dating was performed by laser-ablation-inductively coupled plasma-mass spectrometry (LA-ICP-MS) at the State Key Laboratory of Earthquake Dynamics, Institute of Geology, China Earthquake Administration. The Resolution M50-LR laser-ablation system equipped with a 193 nm excimer ArF laser-ablation system was used, which is connected with an Agilent 7900 ICP-MS. Helium was used as the carrier gas to enhance the transport efficiency of the ablated material. The helium carrier gas inside the ablation cell was mixed with argon gas before entering the ICP to maintain stable and optimum excitation conditions. The analyses were conducted with a beam diameter of 26 μm with analysis time including ~30 s background measurement with the laser off and a 60 s measurement of peak intensity. Harvard Zircon 91500 was used as an external standard, with a recommended $^{206}Pb/^{238}U$ age of (1 065.4±0.6) Ma (Wiedenbeck et al., 1995). Zircon standard GJ-1, with a recommended $^{206}Pb/^{238}U$ age of (608±0.4) Ma (Jackson et al., 2004) was used as the second external standard and analyzed as an unknown sample to verify the accuracy of the method. The glass standard NIST 610 was used as an internal standard to optimize the machine. The trace element concentrations were calibrated using ^{29}Si as an internal standard and NIST 610 as external reference material for zircon. Isotope ratio and trace elemental raw data were processed with the Glitter 4.0 (Macquarie University, Australia) program. The $^{206}Pb/^{238}U$ and $^{207}Pb/^{206}Pb$ ages were finally adopted for zircons younger and older than 1 000 Ma, respectively. For statistical purposes, ages that display more than ±10% discordance were rejected in this study. The weighted mean U-Pb ages and age spectra plots were made using ISOPLOT (version 3.0).

3.2 *Zircon Hf isotope analysis*

In situ Hf isotopic analyses were conducted at the Analytical Laboratory Beijing Research Institute of Uranium Geology, using a Coherent Geolas 193 laser-ablation system and a Nu Plasma Ⅱ multi-collector inductively coupled plasma mass spectrometry (MC-ICP-MS). The spot diameter and pulse rate of the laser were 44 μm and 10 Hz, respectively. The energy density was 10 J/cm^2. Helium was applied as the carrier gas and merged with argon (make-up gas) via a T-connector. Small amounts of nitrogen were added to the make-up gas to improve the sensitivity of Hf isotopes. Harvard zircon 91500 (Blichert-Toft, 2008) was used as an external standard, and Zircon Plešovice (Sláma et al., 2008) was analyzed as unknown during the analyses.

The isobaric interference of ^{176}Lu on ^{176}Hf was corrected by measuring the intensity of the interference-free ^{175}Lu isotope, with a recommended $^{176}Lu/^{175}Lu$ ratio of 0.026 55 (Blichert-Toft et al., 1997). Similarly, the isobaric interference of ^{176}Yb on ^{176}Hf was corrected by measuring the interference-free ^{173}Yb isotope and using a recommended $^{176}Yb/^{173}Yb$ ratio of 0.793 81 (Fisher et al., 2014) to calculate $^{176}Hf/^{177}Hf$ ratios. Applying an exponential fractionation law, the mass fractionations of Hf and Yb were calculated using values of 0.732 5 (Blichert-Toft et al., 1997) for $^{179}Hf/^{177}Hf$ and 1.132 685 for $^{173}Yb/^{171}Yb$ (Fisher et al., 2014), respectively. Because Lu and Yb have similar physicochemical properties, the mass fractionation of Yb was used to correct the mass fractionation of Lu.

The initial Hf isotope ratios are denoted as $\varepsilon Hf(t)$ values that were calculated with the Chondritic Uniform Reservoir (CHUR) at the time of zircon crystallization, and the present-day $^{176}Hf/^{177}Hf$ and $^{176}Lu/^{177}Hf$ ratios of chondrite and depleted mantle of 0.282 77 and 0.033 2, 0.283 25 and 0.038 4, respectively (Blichert-Toft and Albarède, 1997). Initial $^{176}Hf/^{177}Hf$ values were calculated based on ^{176}Lu decay constant of 1.867×10^{-11} a^{-1} reported (Söderlund et al., 2004). The single-stage model Hf ages (T_{DM1}) were calculated relative to the depleted mantle with a present-day $(^{176}Lu/^{177}Hf)_{DM}$=0.038 4 and $(^{176}Hf/^{177}Hf)_{DM}$=0.283 25 (Griffin et al., 2000); the two-stage continental model ages (T_{DM2}) were calculated by projecting the initial $^{176}Hf/^{177}Hf$ of zircon back to the depleted mantle growth curve using $^{176}Lu/^{177}Hf$=0.015 for the average continental crust (Griffin et al., 2002).

3.3 *Whole-rock major and trace element analyses*

Whole-rock major and trace elements were also analyzed at the Analytical Laboratory Beijing Research Institute of Uranium Geology. Major elements were determined using an X-ray fluorescence spectrometer (XRF). Analytical uncertainties were 3% for major elements. Trace elements were analyzed according to the solution ICP-MS technique using a NexION 300D. About 50 mg of powdered sample was dissolved in Telfon bombs using a $HF+HNO_3$ mixture. An internal standard solution containing the single element Rh was used to monitor signal drift during count-

ing. The USGS rock standards (BCR-2 and BHVO-2) and the Chinese national rock standards (GSR-1 and GSR-2) were chosen for calibrating element concentrations of measured samples. Analytical uncertainties were generally <5%.

4 Results

A total of 190 concordant zircon U-Pb ages obtained from the seven samples are listed in Supplementary Table S1. *In situ* Hf isotope data are listed in Supplementary Table S2. Whole-rock major, trace element compositions from six of the samples are presented in Supplementary Table S3.

4.1 *Zircon U-Pb geochronology*

The zircon grains are euhedral-subhedral in shape, display fine-scale oscillatory growth zoning (Fig. 2), and have high Th/U ratios (0.11–1.58) (Fig. 3 and Supplementary Table S1), indicating a magmatic origin (Koschek, 1993; Belousova et al., 2002).

The U-Pb concordia plots and weighted mean age results are presented in Fig. 4. Twenty-seven effective data were obtained from Sample Q2, with ages varying from 246.2 Ma to 2 538.6 Ma. Among them, eighteen grains define a late Permian weighted mean $^{206}Pb/^{238}U$ ages of (253±3.4) Ma (MSWD=6.0), while the other nine grains yield significantly higher ages of 2 538.6 Ma to 2 166.6 Ma (Neoarchean-Paleoproterozoic) (Fig. 4a). Twenty-nine effective data from Sample Q9 yield an early Cretaceous age with a weighted mean $^{206}Pb/^{238}U$ age of (120.6±0.6) Ma (MSWD=1.13) (Fig. 4b). Twenty-two effective data points from Sample Q12 define a middle Permian age, with a weighted mean $^{206}Pb/^{238}U$ age of (270.0±1.2) Ma (MSWD=0.85) (Fig. 4c). Thirty-two effective data from Sample Q18 produce a Middle Triassic age with a weighted mean $^{206}Pb/^{238}U$ age of (237.9±0.99) Ma (MSWD=0.17) (Fig. 4d). Twenty-seven effective data from Sample Q1 yield a weighted mean $^{206}Pb/^{238}U$ ages of (228.9±1.0) Ma (MSWD=0.15) (Fig. 4e). Besides the late Triassic grains, two Neoarchean zircon grains with $^{207}Pb/^{206}Pb$ ages of (2 558±17) Ma and (2 708±17) Ma were also identified in Sample Q1 (Fig. 4e). Eight effective data from Sample Q5 yield a middle Triassic age with a weighted mean $^{206}Pb/^{238}U$ age of (246.2±3.4) Ma (MSWD=5.3) (Fig. 4f). Thirty-three effective data from Sample Q6 produce a middle Triassic age with a weighted mean $^{206}Pb/^{238}U$ age of (239.3±0.96) Ma (MSWD=0.43) (Fig. 4g).

In summary, the 190 zircons from the studied samples yield U-Pb ages varying from 119 Ma to 2 708 Ma, including six Neoarchean (from 2 516.6 Ma to 2 708 Ma) and five Paleoproterozoic ages (from 2 166.6 Ma to 2 434.3 Ma). The Late Paleozoic-Mesozoic weighted mean ages of the 7 analyzed samples are interpreted as the crystallization age, while the significantly older Neoarchean to Paleoproterozoic ages is reflective of xenocryst grains.

4.2 *In situ zircon Hf isotopes*

The 190 zircon grains have variable initial $^{176}Hf/^{177}Hf$ ratios of 0.281 190 to 0.282 965, corresponding to $\varepsilon Hf(t)$ values of –11.1 to 11.3, with one-stage Hf Model ages (T_{DM1}) ranging from 2 841 Ma to 421Ma, and two-stage Hf Model ages (T_{DM2}) ranging from 3 127 Ma to 557 Ma (Fig. 5a).

For Sample Q2, eighteen late Late Paleozoic-Early Mesozoic zircons of 270–246.2 Ma possess $\varepsilon Hf(t)$ values from 1.6 to 11.3, corresponding to T_{DM1} of 903–443 Ma, and T_{DM2} of 1 180 Ma to 557 Ma. The other nine Neoarchean-Paleoproterozoic zircons with a large age range of 2 538.6–2 166.6 Ma, have $\varepsilon Hf(t)$ values ranging from –6.3 to 3.9, with T_{DM2} of 3 127 Ma to 2 786 Ma. Zircon grains from Sample Q9 have $\varepsilon Hf(t)$ values of 3.8 to 9.4, corresponding to T_{DM1} of 643–421 Ma and T_{DM2} age of 937–581 Ma. Sample Q12 presents $\varepsilon Hf(t)$ values from –6.6 to –3.4, corresponding to T_{DM2} of 1 710–1 504 Ma. Zircon grains from Sample Q18 show $\varepsilon Hf(t)$ values ranging from –6.9 to –0.8, corresponding to T_{DM2} of 1 704–1 314 Ma. For Sample Q1, excluding two Neoar-

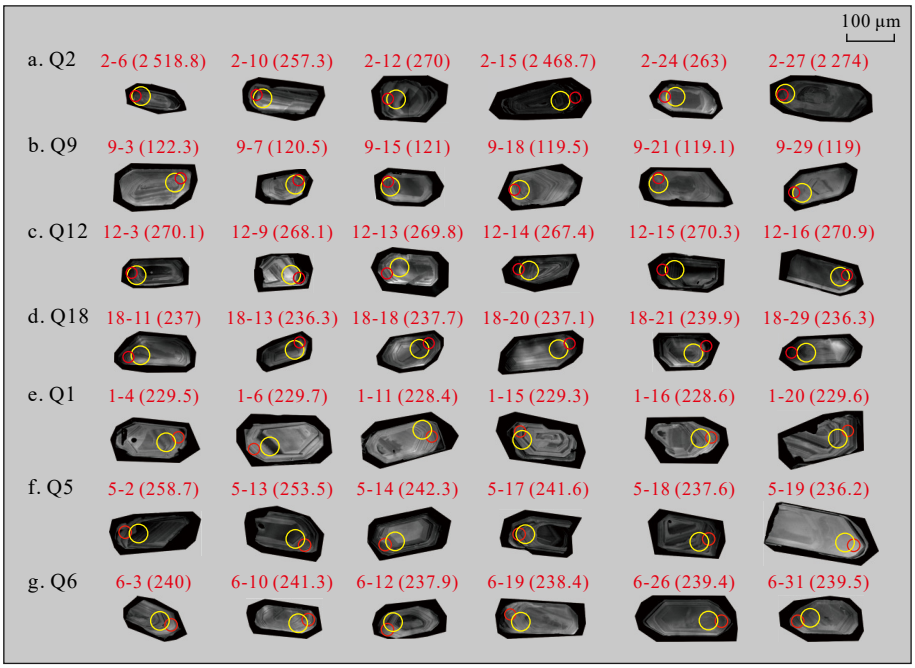

Fig. 2. Cathodoluminescence (CL) images of representative detrital zircons were analyzed for the U-Pb ages. The red and yellow circles denote the analytical spots for the LA-ICP-MS U-Pb dating and Lu-Hf isotopes, respectively. Numbers near the circles indicate are spot number (U-Pb ages), $^{207}Pb/^{206}Pb$ ages are selected for zircons older than 1 000 Ma, and $^{206}Pb/^{238}U$ ages for zircons less than 1 000 Ma.

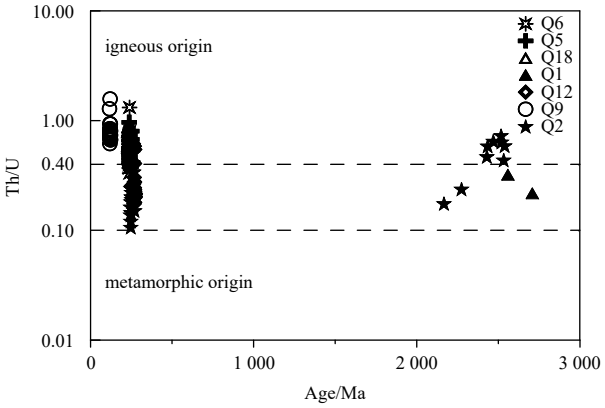

Fig. 3. The Th/U ratio of zircon grains with U-Pb ages. Most of them have high Th/U ratios ranging from 0.11 to 1.58, together with the euhedral-subhedral in shape and fine-scale oscillatory growth zoning in CL images (Fig. 2), suggesting igneous origin (Belousova et al., 2002; Koschek, 1993).

chean spots of 2 708.1 Ma and 2 558.5 Ma, with positive εHf(t) values of 3.9 and 1.5, corresponding to T_{DM1} of 2 922 Ma and 2 951 Ma, respectively, other twenty-seven Early Mesozoic zircons of 226.4–230.8 Ma present εHf(t) values ranging from –1.7 to 4.1, corresponding to T_{DM2} of 1 365–999 Ma. The determined εHf(t) values of Sample Q5 spread between –8.5 and 1.6, correspondingly, their T_{DM2} range from 1 809 Ma to 1 165 Ma. Zircon grains from Sample Q6 have εHf(t) values of –11.1 to 5.1, with the T_{DM2} of 1 965–942 Ma.

Excluding the Neoarchean-Paleoproterozoic zircon grains, grains from Sample Q12 with an emplacement age of ~270.0 Ma, have εHf(t) values varying from –6.6 to –3.4 (Fig. 5b), corresponding T_{DM2} ranging from 1 710 Ma to 1 504 Ma, suggesting the reworking of crustal components older than 1 504 Ma. Grains from samples with emplacement age of ~253–228.9 Ma have εHf(t) values varying from –11.1 to 11.3, the corresponding T_{DM2} of 1 965.1–557.3 Ma, implying the melting of ancient crustal components and the possible addition of juvenile material. The εHf(t) values for grains from Sample Q9, with of emplacement age of ~120.6 Ma, vary from 3.8 to 9.4, and their corresponding T_{DM1} range from 643 Ma to 421 Ma, indicating the addition of juvenile mantle-derived material.

4.3 *Whole-rock major and trace element compositions*

The six samples exhibit contents of SiO_2 (44.47%–68.05%), Al_2O_3 (11.35%–16.07%), MgO (0.42%–4.28%), Fe_2O_3 (1.63%–7.02%), and CaO (1.76%–11.70%). They plot into the monzodiorite, monzonite, and quartz monzonite fields in the TAS classification diagram (Fig. 6a). To be noticed, the diagrams generated based on the Whole-rock major and trace element compositions here and after are just for reference since the LOI is relatively high (5.72–15.25).

The granitoids have A/CNK values of 0.37–1.03, i.e. metaluminous (Fig. 6b). They range across high K calc-alkaline series and shoshonite series (Fig. 6c). In the Harker diagrams, P_2O_5 decreases with increasing SiO_2 (Fig. 6d), Y and Th increase with increasing Rb (Figs 6e and f). The granodiorites and quartz monzonites have moderate rare earth element (REE) contents (100.0×10^{-6}–172.2×10^{-6}). Chondrite-normalized REE diagrams for these granitoids show light REE (LREE) enrichment and Eu negative anomalies (Fig. 7a). In the primitive mantle-normalized variation diagrams, all the rocks show distinct negative anomalies in Nb, Ta, P, Zr, and Ti, and positive anomalies in K, Pb (Fig. 7b).

5 Discussion

5.1 *Geochronological framework of the basement granitoids on northern SCS*

The newly acquired U-Pb ages of the basement granitoids in the QDNB in this study indicate Middle to Late Permian (270–253 Ma), Triassic (246.2–228.9 Ma), and Early Cretaceous (120.6 Ma) crystallization ages. These new data, in combination with published K-Ar dating results (Qiu et al., 1996; Li et al., 1999a), and U-Pb ages from northern SCS basins (Shi et al., 2011; Xu et al., 2016; 2017; Cui et al., 2021), range from 270 Ma to 70.5 Ma, falling into three groups, i.e. 270–196 Ma, 162–142 Ma, and 137–71 Ma (Fig. 9). This dataset defines the Indosinian, Early Yanshanian, and Late Yanshanian tectono-magmatism, which are widespread in the SCB (Zhou et al., 2006; Li and Li, 2007; Wang et al., 2013; and references therein).

5.2 *Unexposed Paleozoic and pre-Proterozoic components beneath northern SCS*

Studies in the SCS Basin basement are of crucial significance in structural geology and regional geodynamic reconstruction (Braitenberg et al., 2006). However, the age and distribution of the basement rocks remain enigmatic. Based on comprehensive gravity-seismic-magnetic inversion analyses, it was previously postulated that there are four lithospheric layers in the basement of the northern SCS basin, which were assigned pre-Sinian, Sinian-early Paleozoic, late Paleozoic, and Mesozoic ages (Sun et al., 2014). Extrapolation suggested that the basement for the QDNB and western Zhujiang River Mouth Basin east of Hainan Island is dominated by Paleozoic strata (Liu et al., 2011; Sun et al., 2014). The basement of the Xisha area has a previously reported Precambrian Rb-Sr isochron age (Qin, 1987). However, updated U-Pb age determinations suggest a Late Jurassic amphibole plagiogneiss basement for the Xisha area, which was later intruded by Early Cretaceous plutons (Zhu et al., 2017). In particular, recent works also suggest that the northern SCS is composed of a uniform Mesozoic basement while the Precambrian rocks are only constricted along the Red River Fault Zone (Zhou et al., 2002; Cui et al., 2021). Therefore, it remains unclear whether the northern South China Sea basin has ever been floored by Paleozoic or even Precambrian components.

Two samples with weighted average ages of (253±3.4) Ma (MSWD=6.0) (Sample Q2) and (270.0±1.2) Ma (MSWD=0.85) (Sample Q12) in this study demonstrated that there may be Paleozoic components beneath the northern SCS. In addition, six Neoarchean ages (2 708.1–2 516.6 Ma) were obtained in the study (Supplementary Table S1, Fig. 10a). They have positive εHf(t) of 0.6 to 3.9 and yield similar T_{DM1} and T_{DM2} ages (2 841–2 690 Ma and 2 922–2 786 Ma), suggesting that there may have been some addition of juvenile material in Mesoarchean-Neoarchean. Five Paleoproterozoic zircons with the age of 2 468.7 Ma to 2 166.6 Ma have εHf(t) values of –6.3 to 2.2 and yield T_{DM2} of 3 127 Ma to 2 838 Ma, implying the melting of ancient crustal components older than 2.9 Ga and the possible addition of juvenile material in Mesoarchean. These data are likely to imply that there might also be pre-Proterozoic components beneath the northern SCS.

Due to scarce borehole penetration, the northern SCS Basin basement is hard to trace and data here indeed is insufficient to support the existence of such old basement components. Under such circumstances, achievements from neighboring areas may offer clues. A compilation of 812 Precambrian U-Pb ages of xenocrystic/inherited zircons from the Cathaysia Block presents a

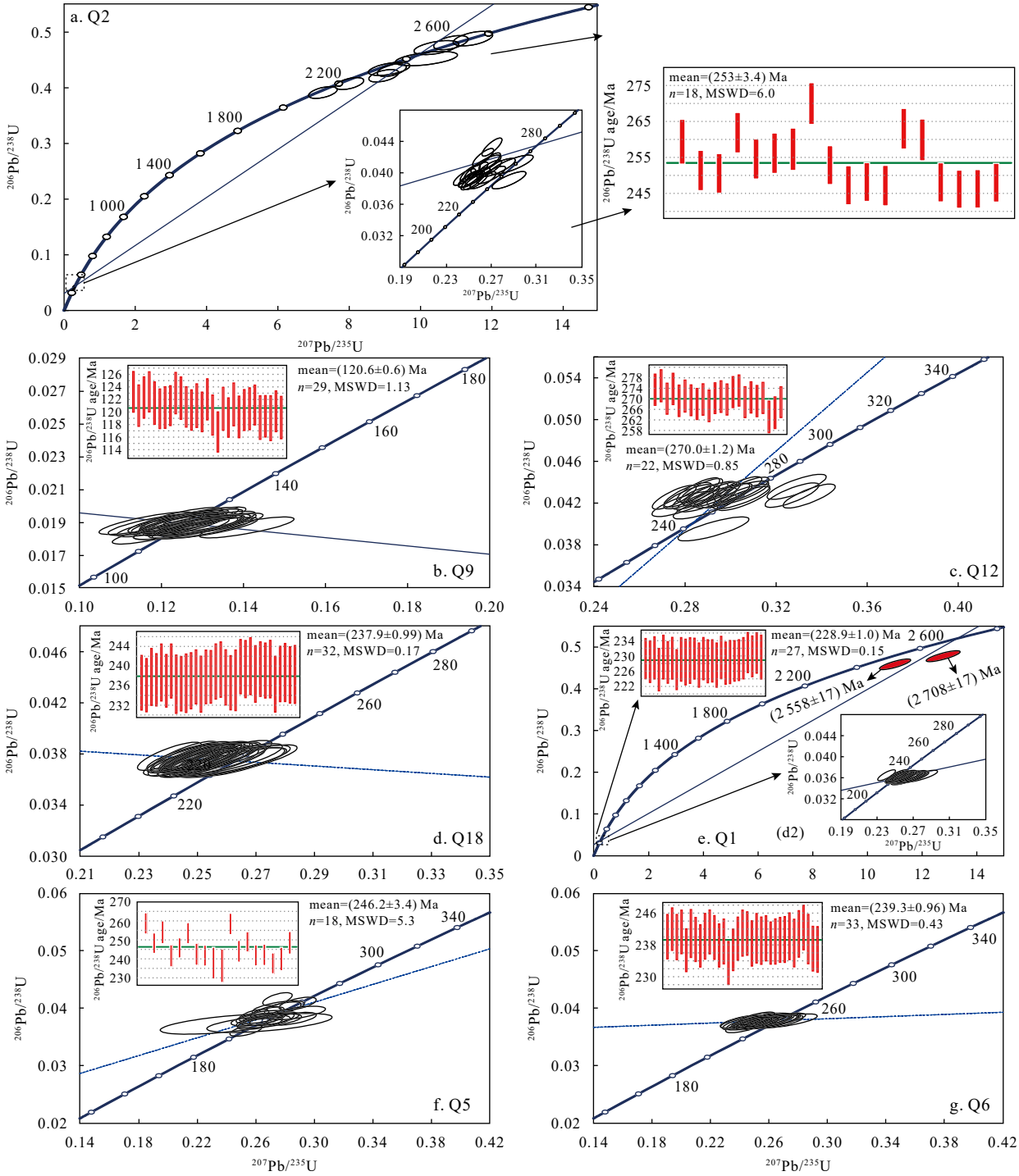

Fig. 4. Zircon U-Pb concordia plots and weighted mean ages for basement granitoid in the Qiongdongnan Basin.

wide age range between 3 866 Ma and 545 Ma, with three major populations of 2 700–2 400 Ma, 2 050–1 750 Ma, and 1 100–700 Ma, peaking at 2 470 Ma, 1 850 Ma, and 715 Ma, respectively (Fig. 10b). Although there are no exposed Archean rocks, Archean ages found in xenocrystic/inherited zircons in different parts of the Cathaysia Block may imply the possible presence of Archean crust beneath this block (Fig. 10b) (Jiang et al., 2020; Wang et al., 2020a, b and references therein). In addition, xenocrystic/inherited zircons U-Pb ages (Jiang et al., 2020; Wang et al., 2020a, 2020b), combined with the Paleoproterozoic outcrops discovered in the Badu Group (Yu et al., 2012), as well as the Paleoproterozoic source of late Mesozoic volcanic in the Yandangshan area (Yan et al., 2016), probably suggests a widespread existence of Paleoproterozoic basement beneath eastern Cathaysia. It is supposed that the northern SCS Basin basement was the southward extension of the Cathaysia Block (Hayes and Nissen, 2005; Lei and Ren, 2016; Xu et al., 2013). Thus, the identification of Paleoproterozoic to Neoarchean zircons in this study (Fig. 10a) might provide clues to the potential existence of the pre-Proterozoic components beneath northern SCS, though much more reliable rock information from the unexposed basement is necessary to get this statement.

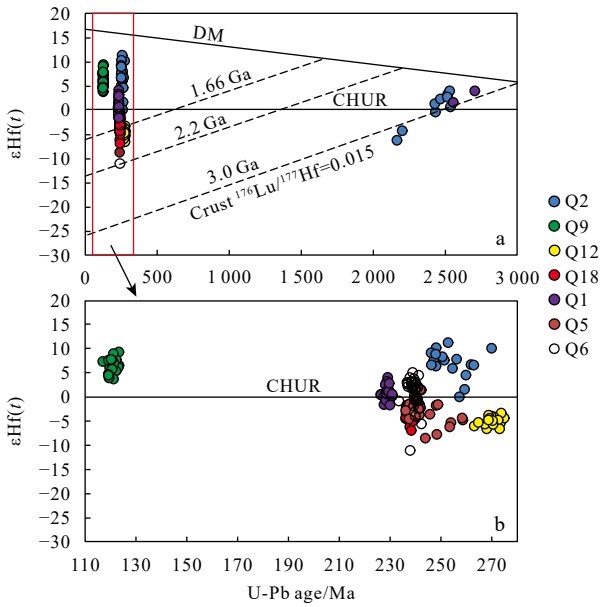

Fig. 5. εHf (*t*) values versus U-Pb ages, illustrating the comparison of εHf (*t*) of zircon from the basement granitoids in the Qiongdongnan Basin. DM: depleted mantle; CHUR: Bulk earth (chondritic uniform reservoir). Hf-isotope evolution line for depleted mantle is after Griffin et al. (2000). The dotted lines in a represent average crust $^{176}Lu/^{177}Hf$=0.015 (Griffin et al., 2002).

5.3 *Tectonic affinity of the basement granitoids and tectonic implication*

While there is a consensus that the Jurassic to late Cretaceous Yanshanian magmatism in southeastern China has resulted from the subduction of the Pale-Pacific Plate (Li and Li, 2007; He and Xu, 2012; Liu et al., 2012), the tectonic setting of the Late Permian to Triassic magmatism remain controversial due to the superimposed effect of Palaeo-Pacific and Palaeo-Tethys tectonic regimes. Some works have interpreted the Late Permian to Triassic magmatism as being caused by continent-continent collision related to the closure of the Paleo-Tethyan ocean to the southwest of South China (Zhou et al., 2006; Yan et al., 2007; Yan et al., 2014, 2017). The alternative model proposed that this period may record the initiation of a continental arc resulting from the subduction of the Paleo-Pacific Plate beneath the Eurasian plate including Hainan Island (Li and Li, 2007).

The plot of Ga/Al versus Nb is an effective discriminator that allows the separation of A-type granite from other types (Whalen et al., 1987). The granitoids from the QDNB basement have low Nb (less than 14.5×10^{-6}) and low Ga/Al ratios (less than 2.2), placing them in the I- and S-type field (Fig. 8a). Moreover, the A/NK versus A/CNK plot (Fig. 6b), the negative correlations between SiO_2 and P_2O_5 (Fig. 6d), the positive correlation between Y and Rb (Fig. 6e), and the positive correlation between Th and Rb (Fig. 6f) further defined them to be the I-type. They mainly belong to the high K calc-alkaline series (Fig. 6c). K-rich calc-alkaline granites are preserved in various geodynamic environments, where transition happened from a compressional regime to an extensional regime, including subduction and active continental margin or post-collisional uplift (Barbarin, 1999). In the plots of Rb vsrsus Y + Nb (Fig. 8b) (Pearce et al., 1984), Sr/Y vsrsus Y (Defant et al., 2002) (Fig. 8c), and $(La/Yb)_N$ vsrsus $(Yb)_N$ (Martin, 1993) (Fig. 8d), granitoids in this study plot in the field of the volcanic arc. Moreover, the rocks exhibit well-defined negative Nb, Ta, and Ti anomalies (Fig. 7b), typical of subduction-related magmas (Sajona et al., 1993).

In addition, studies on Permian to Triassic gneissic granites in central Hainan Island, which is next to the Qiongdongnan Basin, show well-developed schistosity, with dominant NNE–NE strike

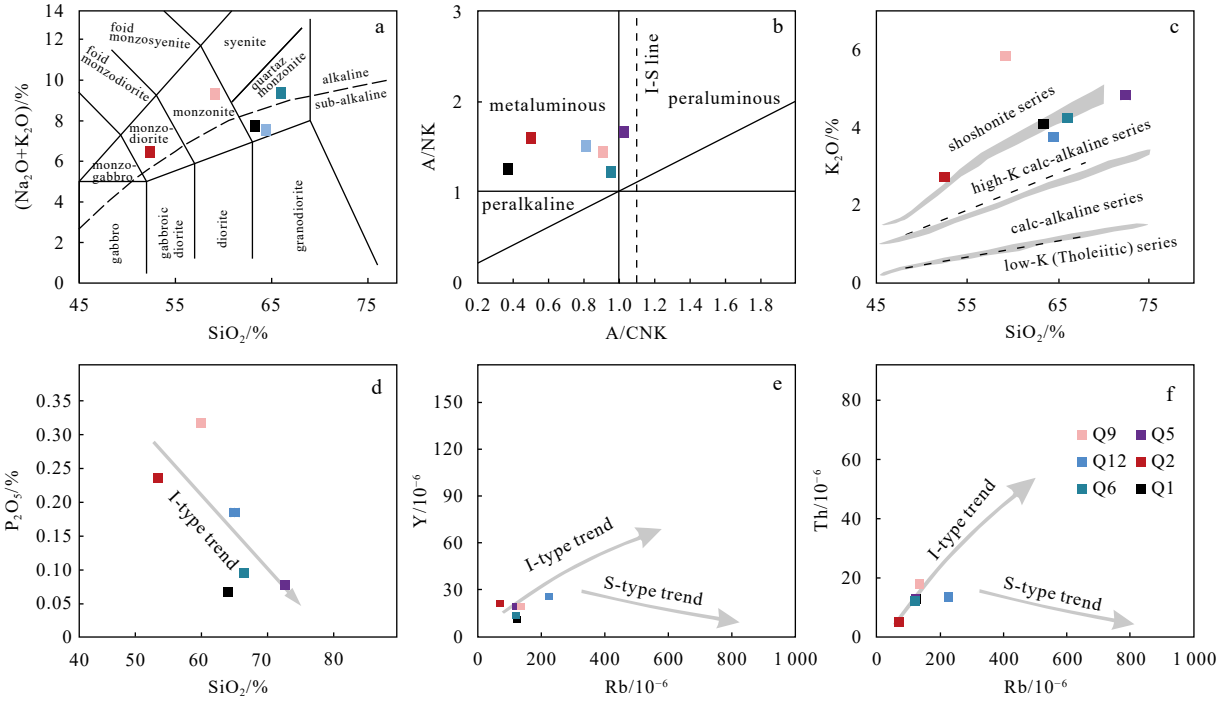

Fig. 6. Geochemical features of the basement granitoids from the Qiongdongnan Basin. a. SiO_2 versus K_2O+Na_2O (Middlemost, 1994), b. A/CNK versus A/NK diagram (Maniar and Piccoli, 1989), c. SiO_2 versus K_2O scheme, where the subdivisions from low-K tholeiite, calc-alkaline, high-K calc-alkaline to shoshonite are from Rickwood (1989), d. SiO_2 versus P_2O_5, e. Rb versus Y, and f. Rb versus Th plot for identification of I-type from S-type granite (Chappell, 1999).

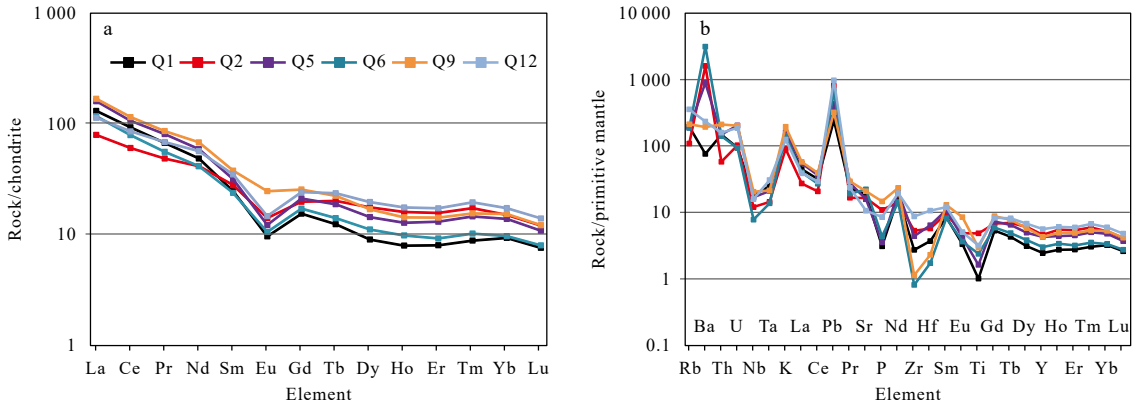

Fig. 7. Chondrite-normalized REE patterns (a), and primitive mantle normalized trace element patterns (b), of basement granitoids from the Qiongdongnan Basin. Chondrite and primitive mantle values are from Sun and McDonough (1989).

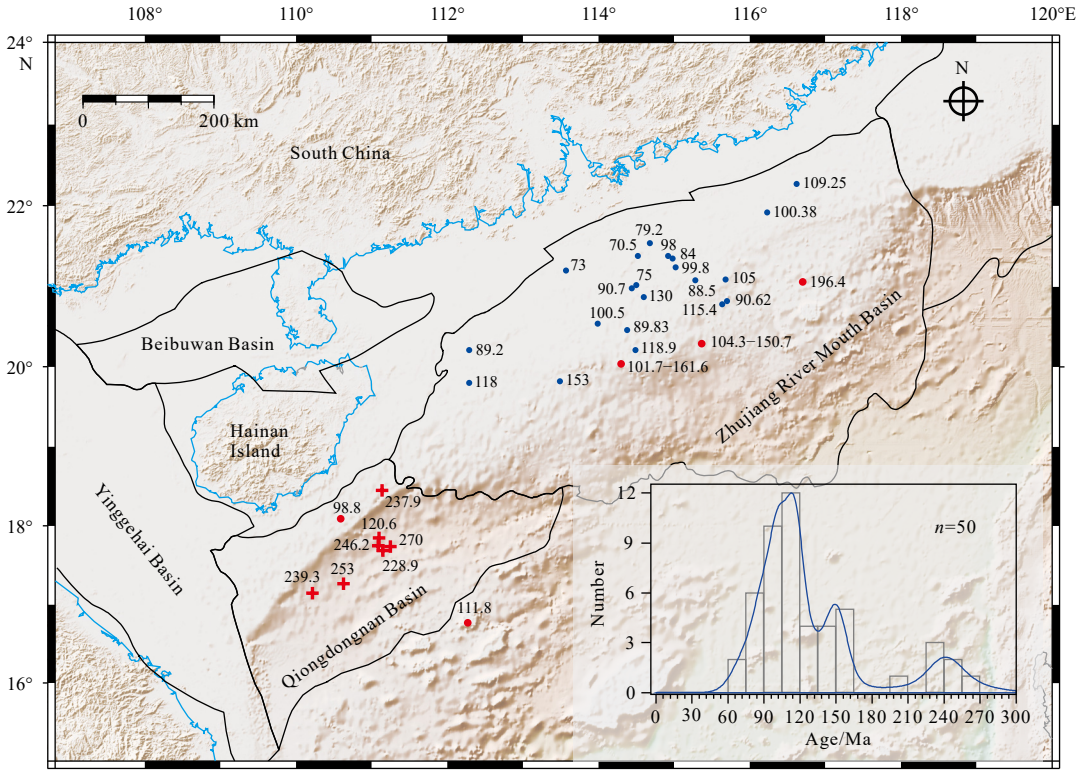

Fig. 8. Distribution of and age summary of granitoids in northern South China Sea Basin. Crosses denote samples analyzed in this study, while circles present ages reported in previous studies (blue ones, K-Ar ages from Li et al. (1999a) and Qiu et al. (1996); red ones, U-Pb ages from Cui et al. (2021), Shi et al. (2011) and Xu et al. (2016, 2017). Black curves denote basin boundary.

directions (e.g., Li et al., 2005b; Li et al., 2006; Xie et al., 2006), and these granitic plutons all exhibit NE–SW extension, which is incompatible with the NW-trending Paleo-Tethyan tectonic regime. Moreover, Permian magmatism reported in the Hainan Island (267–245 Ma) (Li et al., 2006; Shen et al., 2018), southeastern Korea (257–250 Ma; Cheong et al., 2014; Yi et al., 2012), and the Hida Belt of Japan (256–250 Ma; Horie et al., 2010; Zhao et al., 2013), have been identified as arc-related magmatism ascribed to subduction of the Paleo-Pacific Plate beneath eastern Asia.

From the discussion above, we prefer that the granitoids described in this study occurred in a volcanic arc setting induced by the subduction of the Paleo-Pacific Plate, although the mechanism may be more complicated and unclear.

6 Conclusions

Based on an integrated study of zircon U-Pb geochronology, Hf isotopes, and whole-rock major and trace elements analysis on basement granitoids of the Qiongdongnan Basin, as well as previous age data on the northern South China Sea, we draw the following major conclusions:

(1) Granitoids ages in the northern South China Sea cover a range of 270 Ma to 70.5 Ma, falling into three age groups of 270–196 Ma, 162–142 Ma, and 137–71 Ma, which correspond to the Indosinian, Early Yanshanian, and Late Yanshanian tectonomagmatism in the South China Block.

(2) Besides the Late Paleozoic to Mesozoic basement rocks of the northern South China Sea, the old grain ages of 2 708–2 166.6 Ma reals the potential presence of the Neoarchean-Paleoprotero-

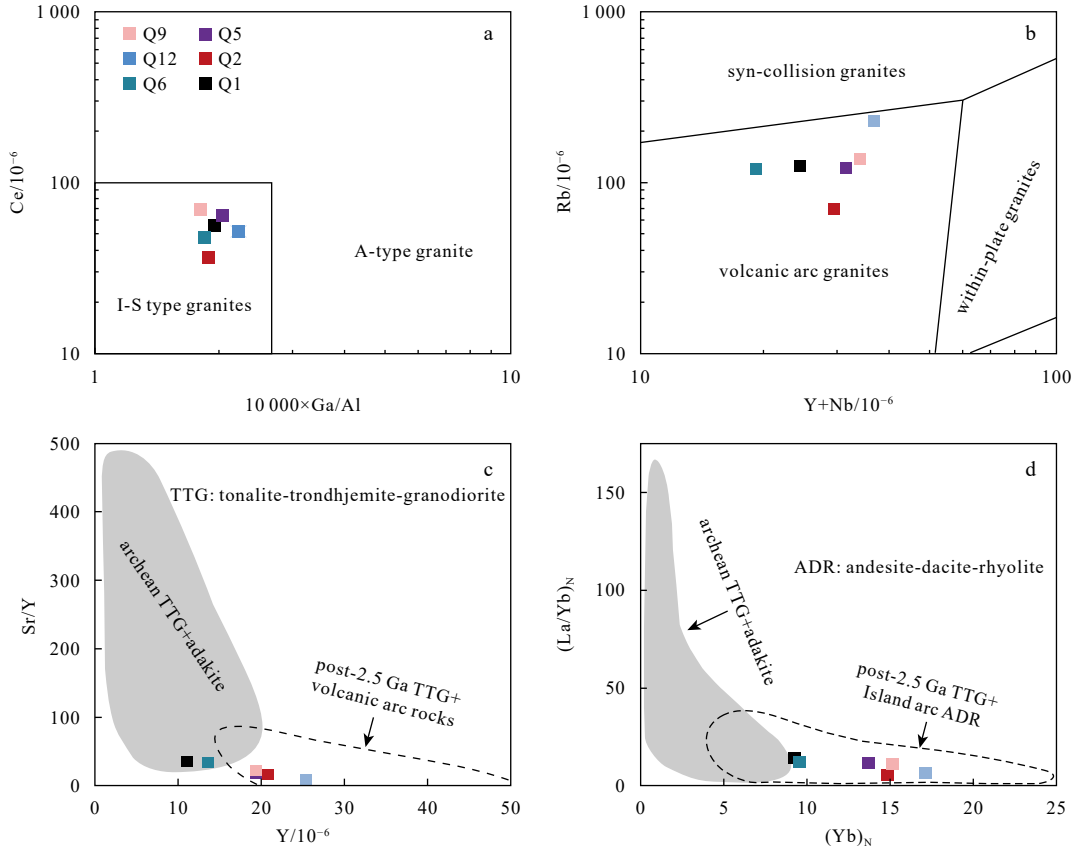

Fig. 9. Ga×10 000/Al versus Ce plot for identification of A-type granite from I- and S-type granites (Whalen et al., 1987) (a), Y+Nb versus Rb plot for discriminating syn-collisional granite, volcanic-arc granite, within-plate granite, and ocean-ridge granite (Pearce et al., 1984) (b), Y versus Sr/Y plot (Defant et al., 2002) (c), and $(Yb)_N$ versus $(La/Yb)_N$ plot (Martin, 1993) (d). TTG: tonalite-trondhjemite-granodiorite; ADR: andesite-dacite-rhyolite.

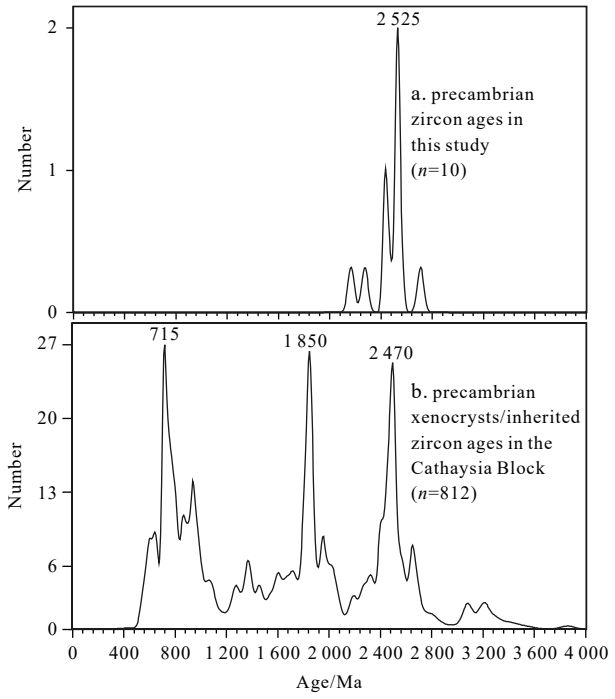

Fig. 10. Probability density plots of precambrian U-Pb ages for zircons in this study (a) and xenocrystic/inherited zircon ages in the cathaysia block (b). Data source for references (Wang et al., 2020a, b; Jiang et al., 2020) .

zoic components beneath the northern South China Sea.

(3) The Late Permian-Early Cretaceous granitoids of the Qiongdongnan Basin belong to I-type granites, with volcanic arc affinity. Typical signatures of subduction-related magmas suggest that the granitoids likely resulted from the subduction of the Paleo-Pacific Plate.

Acknowledgements

We are grateful to Jianzhang Pang and Guanggao Zheng for their help during the analyses of the samples.

References

Barbarin B. 1999. A review of the relationships between granitoid types, their origins and their geodynamic environments. Lithos, 46(3): 605–626, doi: 10.1016/S0024-4937(98)00085-1

Barckhausen U, Engels M, Franke D, et al. 2014. Evolution of the South China Sea: Revised ages for breakup and seafloor spreading. Marine and Petroleum Geology, 58: 599–611, doi: 10.1016/j.marpetgeo.2014.02.022

Belousova E, Griffin W, O'Reilly S Y, et al. 2002. Igneous zircon: trace element composition as an indicator of source rock type. Contributions to Mineralogy and Petrology, 143(5): 602–622, doi: 10.1007/s00410-002-0364-7

Blichert-Toft J. 2008. The Hf isotopic composition of zircon reference material 91500. Chemical Geology, 253(3–4): 252–257

Blichert-Toft J, Albarède F. 1997. The Lu-Hf isotope geochemistry of chondrites and the evolution of the mantle-crust system. Earth and Planetary Science Letters, 148(1–2): 243–258

Blichert-Toft J, Chauvel C, Albarède F. 1997. Separation of Hf and Lu for high-precision isotope analysis of rock samples by magnet-

ic sector-multiple collector ICP-MS. Contributions to Mineralogy and Petrology, 127(3): 248–260, doi: 10.1007/s004100050278

Braitenberg C, Wienecke S, Wang Y. 2006. Basement structures from satellite-derived gravity field: South China Sea ridge. Journal of Geophysical Research: Solid Earth, 111(B5): B05407

Cao L C, Jiang T, Wang Z F, et al. 2015. Provenance of Upper Miocene sediments in the Yinggehai and Qiongdongnan basins, northwestern South China Sea: Evidence from REE, heavy minerals and zircon U-Pb ages. Marine Geology, 361: 136–146, doi: 10.1016/j.margeo.2015.01.007

Chappell B W. 1999. Aluminium saturation in I- and S-type granites and the characterization of fractionated haplogranites. Lithos, 46(3): 535–551, doi: 10.1016/S0024-4937(98)00086-3

Chen Chenghong, Lee Chi-Yu, Shinjo R. 2008. Was there Jurassic paleo-Pacific subduction in South China?: Constraints from $^{40}Ar/^{39}Ar$ dating, elemental and Sr-Nd-Pb isotopic geochemistry of the Mesozoic basalts. Lithos, 106(1–2): 83–92

Cheong C S, Kim N, Kim J, et al. 2014. Petrogenesis of Late Permian sodic metagranitoids in southeastern Korea: SHRIMP zircon geochronology and elemental and Nd-Hf isotope geochemistry. Journal of Asian Earth Sciences, 95: 228–242, doi: 10.1016/j.jseaes.2014.06.005

Cui Yuchi, Shao Lei, Li Zhengxiang, et al. 2021. A Mesozoic Andean-type active continental margin along coastal South China: New geological records from the basement of the northern South China Sea. Gondwana Research, 99: 36–52, doi: 10.1016/j.gr.2021.06.021

Cullen A, Reemst P, Henstra G, et al. 2010. Rifting of the South China Sea: new perspectives. Petroleum Geoscience, 16(3): 273–282, doi: 10.1144/1354-079309-908

Defant M J, Xu Jifeng, Kepezhinskas P, et al. 2002. Adakites: some variations on a theme. Acta Petrologica Sinica, 18(2): 129–142

Fisher C M, Vervoort J D, Hanchar J M. 2014. Guidelines for reporting zircon Hf isotopic data by LA-MC-ICPMS and potential pitfalls in the interpretation of these data. Chemical Geology, 363: 125–133, doi: 10.1016/j.chemgeo.2013.10.019

Griffin W L, Pearson N J, Belousova E, et al. 2000. The Hf isotope composition of cratonic mantle: LAM-MC-ICPMS analysis of zircon megacrysts in kimberlites. Geochimica et Cosmochimica Acta, 64(1): 133–147, doi: 10.1016/S0016-7037(99)00343-9

Griffin W L, Wang X, Jackson S E, et al. 2002. Zircon chemistry and magma mixing, SE China: *In-situ* analysis of Hf isotopes, Tonglu and Pingtan igneous complexes. Lithos, 61(3–4): 237–269

Hayes D E, Nissen S S. 2005. The South China sea margins: Implications for rifting contrasts. Earth and Planetary Science Letters, 237(3–4): 601–616

He Zhenyu, Xu Xisheng. 2012. Petrogenesis of the Late Yanshanian mantle-derived intrusions in southeastern China: Response to the geodynamics of paleo-Pacific plate subduction. Chemical Geology, 328: 208–221, doi: 10.1016/j.chemgeo.2011.09.014

Horie K, Yamashita M, Hayasaka Y, et al. 2010. Eoarchean-Paleoproterozoic zircon inheritance in Japanese Permo-Triassic granites (Unazuki area, Hida Metamorphic complex): unearthing more old crust and identifying source terrranes. Precambrian Research, 183(1): 145–157, doi: 10.1016/j.precamres.2010.06.014

Huang Baojia, Tian Hui, Li Xushen, et al. 2016. Geochemistry, origin and accumulation of natural gases in the deepwater area of the Qiongdongnan Basin, South China Sea. Marine and Petroleum Geology, 72: 254–267, doi: 10.1016/j.marpetgeo.2016.02.007

Jackson S E, Pearson N J, Griffin W L, et al. 2004. The application of laser ablation-inductively coupled plasma-mass spectrometry to *in situ* U–Pb zircon geochronology. Chemical Geology, 211(1–2): 47–69

Jiang Changhong, Wang Xiaolei, Wang Shuo, et al. 2020. Paleoproterozoic basement beneath the Eastern Cathaysia Block revealed by zircon xenocrysts from late Mesozoic volcanics. Precambrian Research, 350: 105922, doi: 10.1016/j.precamres.2020.105922

Koschek G. 1993. Origin and significance of the SEM cathodoluminescence from zircon. Journal of Microscopy, 171(3): 223–232, doi: 10.1111/j.1365-2818.1993.tb03379.x

Lei Chao, Ren Jiaye. 2016. Hyper-extended rift systems in the Xisha Trough, northwestern South China Sea: Implications for extreme crustal thinning ahead of a propagating ocean. Marine and Petroleum Geology, 77: 846–864, doi: 10.1016/j.marpetgeo.2016.07.022

Li Zhengxiang. 1998. Tectonic history of the major east asian lithospheric blocks since the mid-proterozoic—a synthesis. In: Flower M F J, Chung Sun-Lin, Lo Ching-Hua, et al. Mantle Dynamics and Plate Interactions in East Asia. Washington, DC, USA: American Geophysical Union

Li Jianhua, Dong Shuwen, Cawood P A, et al. 2018. An Andean-type retro-arc foreland system beneath northwest South China revealed by SINOPROBE profiling. Earth and Planetary Science Letters, 490: 170–179, doi: 10.1016/j.epsl.2018.03.008

Li Zhengxiang, Li Xianhau. 2007. Formation of the 1300-km-wide intracontinental orogen and postorogenic magmatic province in Mesozoic South China: a flat-slab subduction model. Geology, 35(2): 179–182, doi: 10.1130/G23193A.1

Li Wuxian, Li Xianhua, Li Zhengxiang. 2005a. Neoproterozoic bimodal magmatism in the Cathaysia Block of South China and its tectonic significance. Precambrian Research, 136(1): 51–66, doi: 10.1016/j.precamres.2004.09.008

Li Xianhua, Li Zhengxiang, Li Wuxian, et al. 2006. Initiation of the Indosinian orogeny in South China: evidence for a Permian magmatic arc on Hainan Island. Journal of Geology, 114(3): 341–353, doi: 10.1086/501222

Li Puping, Liang Huixian, Dai Yiding, et al. 1999a. Origin and tectonic setting of the Yanshanian igneous rocks in the Pearl River Mouth basin. Guangdong Geology (in Chinese), 14(1): 1–8

Li Zhengxiang, Li Xianhua, Kinny P D, et al. 1999b. The breakup of Rodinia: did it start with a mantle plume beneath South China?. Earth and Planetary Science Letters, 173(3): 171–181

Li Sunxiong, Yun Ping, Fan Yuan, et al. 2005b. Zircon U-Pb age and its geological significance for Qiongzhong pluton in Qiongzhong area, Hainan Island. Geotectonica et Metallogenia (in Chinese), 29(2): 227–233, 241

Liu Hailing, Yan Pin, Zhang Boyou, et al. 2004a. Pre-cenozoic basements of the South China Sea and Eastern Tethyan realm. Marine Geology and Quaternary Geology (in Chinese), 24(1): 15–28

Liu Hailing, Yang Tian, Zhu Shufen, et al. 2004b. Tectonic evolution of Cenozoic sedimentary basements in the northwestern South China Sea. Acta Oceanologica Sinica (in Chinese), 26(3): 54–67

Liu Qian, Yu Jinhai, Wang Qin, et al. 2012. Ages and geochemistry of granites in the Pingtan–Dongshan Metamorphic Belt, Coastal South China: New constraints on Late Mesozoic magmatic evolution. Lithos, 150: 268–286, doi: 10.1016/j.lithos.2012.06.031

Liu Xiaofeng, Zhang Daojun, Zhai Shikui, et al. 2015. A heavy mineral viewpoint on sediment provenance and environment in the Qiongdongnan Basin. Acta Oceanologica Sinica, 34(4): 41–55, doi: 10.1007/s13131-015-0648-1

Liu Hailing, Zheng Hongbo, Wang Yanlin, et al. 2011. Basement of the South China Sea area: tracing the Tethyan realm. Acta Geologica Sinica-English Edition, 83(3): 637–655

Lu Baoliang, Su Xiaomeng, Zhang Gongcheng, et al. 2011. Seismic-potential field response characteristics and identification of basement lithology of the northern South China Sea basin. Chinese Journal of Geophysics (in Chinese), 54(2): 563–572

Lu Baoliang, Wang Pujun, Zhang Gongcheng, et al. 2015. Characteristic of regional fractures in South China Sea and its basement tectonic framework. Progress in Geophysics (in Chinese), 30(4): 1544–1553

Maniar P D, Piccoli P M. 1989. Tectonic discrimination of granitoid. GSA Bulletin, 101(5): 635–643, doi: 10.1130/0016-7606(1989)101<0635:TDOG>2.3.CO;2

Martin H. 1993. The mechanisms of petrogenesis of the Archaean continental crust-comparison with modern processes. Lithos, 30(3): 373–388

Meng Miaomiao, Liang Jinqiang, Lu Jing'an, et al. 2021. Quaternary

deep-water sedimentary characteristics and their relationship with the gas hydrate accumulations in the Qiongdongnan Basin, Northwest South China Sea. Deep-Sea Research Part I: Oceanographic Research Papers, 177: 103628, doi: 10.1016/j.dsr.2021.103628

Middlemost E A K. 1994. Naming materials in the magma/igneous rock system. Earth-Science Reviews, 37(3–4): 215–224

Morley C K. 2002. A tectonic model for the Tertiary evolution of strike-slip faults and rift basins in SE Asia. Tectonophysics, 347(4): 189–215, doi: 10.1016/S0040-1951(02)00061-6

Pearce J A, Harris N B W, Tindle A G. 1984. Trace element discrimination diagrams for the tectonic interpretation of granitic rocks. Journal of Petrology, 25(4): 956–983, doi: 10.1093/petrology/25.4.956

Qin Guoqian. 1987. A preliminary study on foraminiferal assemblages of well 1 Xiyong. Xisha Islands and their coral reef formation. Tropic Oceanology (in Chinese), 6(3): 10–20

Qiu Y X, Li P L. 1996. Late Cretaceous-Cenozoic tectonic evolution and nature of continental margin in the northern South China Sea and Taiwan Strait. Guangdong Geology (in Chinese), 11(3): 10–16

Ren Jishun. 1964. A preliminary study on pre-Devonian geotectonic problems of southeastern China. Acta Geologica Sinica (in Chinese), 44(4): 418–431

Rickwood P C. 1989. Boundary lines within petrologic diagrams which use oxides of major and minor elements. Lithos, 22(4): 247–263, doi: 10.1016/0024-4937(89)90028-5

Sajona F G, Maury R C, Bellon H, et al. 1993. Initiation of subduction and the generation of slab melts in western and eastern Mindanao, Philippines. Geology, 21(11): 1007–1010, doi: 10.1130/0091-7613(1993)021<1007:IOSATG>2.3.CO;2

Shen Linwei, Yu Jihai, O'Reilly S Y, et al. 2018. Subduction-related middle Permian to early Triassic magmatism in central Hainan Island, South China. Lithos, 318–319: 158 –175

Shi Hesheng, Xu Changhai, Zhou Zuyi, et al. 2011. Zircon U-Pb dating on granitoids from the Northern South China Sea and its geotectonic relevance. Acta Geologica Sinica-English Edition, 85(6): 1359–1372, doi: 10.1111/j.1755-6724.2011.00592.x

Sláma J, Košler J, Condon D J, et al. 2008. Plešovice zircon—A new natural reference material for U–Pb and Hf isotopic microanalysis. Chemical Geology, 249(1–2): 1–35

Söderlund U, Patchett P J, Vervoort J D, et al. 2004. The ^{176}Lu decay constant determined by Lu-Hf and U-Pb isotope systematics of Precambrian mafic intrusions. Earth and Planetary Science Letters, 219(3–4): 311–324

Su Ao, Chen Honghan, Chen Xu, et al. 2018. New insight into origin, accumulation and escape of natural gas in the Songdong and Baodao regions in the eastern Qiongdongnan basin, South China Sea. Journal of Natural Gas Science and Engineering, 52: 467–483, doi: 10.1016/j.jngse.2018.01.026

Su Nairong, Zeng Lin, Li Pinglu. 1995. Geological features of mesozoic sags in the eastern part of Pearl River Mouth Basin. China Offshore Oil and Gas (Geology) (in Chinese), 9(4): 228–236

Sun Shensu, McDonough W F. 1989. Chemical and isotopic systematics of oceanic basalts: Implications for mantle composition and processes. Geological Society, London, Special Publications, 42(1): 313–345

Sun Xiaomeng, Zhang Xuqing, Zhang Gongcheng, et al. 2014. Texture and tectonic attribute of Cenozoic basin basement in the northern South China Sea. Science China Earth Sciences, 57(6): 1199–1211, doi: 10.1007/s11430-014-4835-2

Tapponnier P, Peltzer G, Armijo R. 1986. On the Mechanics of the Collision Between India and Asia. In: Coward M, Ries A, eds. Collosion Tectonics. London, UK: Geological Society of London Special Publication, 115–157

Taylor B, Hayes D E. 1980. The tectonic evolution of the South China Basin. In: Hayes D E, ed. The Tectonic and Geologic Evolution of Southeast Asian Seas and Islands. Washington, DC, USA: American Geophysical Union, 89–104

Taylor B, Hayes D E. 1983. Origin and history of the South China sea basin. In: Hayes D E, ed. The Tectonic and Geologic Evolution of Southeast Asian Seas and Islands. Geophysics Monographs Series, Washington, DC, USA: American Geophysical Union, 23–56

Wang Kai, Dong Shuwen, Yao Weihua, et al. 2020a. Xenocrystic/inherited Precambrian zircons entrained within igneous rocks from eastern South China: Tracking unexposed ancient crust and implications for late Paleoproterozoic orogenesis. Gondwana Research, 84: 194–210, doi: 10.1016/j.gr.2020.02.015

Wang Yuejun, Fan Weiming, Zhang Guowei, et al. 2013. Phanerozoic tectonics of the South China Block: Key observations and controversies. Gondwana Research, 23(4): 1273–1305, doi: 10.1016/j.gr.2012.02.019

Wang Jialin, Zhang Xinbing, Wu Jiansheng, et al. 2002. Integrated geophysical researches on base texture of Zhujiang River Mouth basin. Journal of Tropical Oceanography (in Chinese), 21(2): 13–22

Wang Tingting, Zheng Jianping, Zhao Huan. 2020b. Unexposed Archean components and complex evolution beneath the Cathaysia Block: Evidence from zircon xenocrysts in the Cenozoic basalts in Leizhou Peninsula, South China. Journal of Asian Earth Sciences, 192: 104268, doi: 10.1016/j.jseaes.2020.104268

Whalen J B, Currie K L, Chappell B W. 1987. A-type granites: Geochemical characteristics, discrimination and petrogenesis. Contributions to Mineralogy and Petrology, 95(4): 407–419, doi: 10.1007/BF00402202

Wiedenbeck M, Corfu P A F, Griffin W L, et al. 1995. Three natural zircon standards for U-Th-Pb, Lu-Hf, trace element and REE analyses. Geostandards Newsletter, 19(1): 1–23, doi: 10.1111/j.1751-908X.1995.tb00147.x

Xie Caifu, Zhu Jinchu, Ding Shijiang, et al. 2006. Identification of Hercynian shoshonitic intrusive rocks in central Hainan Island and its geotectonic implications. Chinese Science Bulletin, 51(20): 2507–2519, doi: 10.1007/s11434-006-2122-0

Xu Changhai, Que Xiaoming, Shi Hesheng, et al. 2013. The southward extension of cathaysia block: evidence from zircon U-Pb dates of borehole volcanics in the northern South China Sea. Acta Geologica Sinica-English Edition, 87(5): 1370–1386, doi: 10.1111/1755-6724.12135

Xu Changhai, Shi Hesheng, Barnes C G, et al. 2016. Tracing a late Mesozoic magmatic arc along the Southeast Asian margin from the granitoids drilled from the northern South China Sea. International Geology Review, 58(1): 71–94, doi: 10.1080/00206814.2015.1056256

Xu Changhai, Zhang Lu, Shi Hesheng, et al. 2017. Tracing an Early Jurassic magmatic arc from South to East China seas. Tectonics, 36(3): 466–492, doi: 10.1002/2016TC004446

Yan Lili, He Zhenyu, Jahn B M, et al. 2016. Formation of the Yandangshan volcanic–plutonic complex (SE China) by melt extraction and crystal accumulation. Lithos, 266–267: 287–308

Yan Quanshu, Metcalfe I, Shi Xuefa. 2017. U-Pb isotope geochronology and geochemistry of granites from Hainan Island (northern South China Sea margin): Constraints on late Paleozoic-Mesozoic tectonic evolution. Gondwana Research, 49: 333–349, doi: 10.1016/j.gr.2017.06.007

Yan Quanshu, Shi Xuefa, Castillo P R. 2014. The late Mesozoic-Cenozoic tectonic evolution of the South China Sea: A petrologic perspective. Journal of Asian Earth Sciences, 85: 178–201, doi: 10.1016/j.jseaes.2014.02.005

Yan Yi, Xia Bin, Lin Ge, et al. 2007. Geochemical and Nd isotope composition of detrital sediments on the north margin of the South China Sea: provenance and tectonic implications. Sedimentology, 54(1): 1–17, doi: 10.1111/j.1365-3091.2006.00816.x

Yi K, Cheong C S, Kim J, et al. 2012. Late Paleozoic to early Mesozoic arc-related magmatism in southeastern Korea: SHRIMP zircon geochronology and geochemistry. Lithos, 153: 129–141, doi: 10.1016/j.lithos.2012.02.007

Zhao Guochun, Cawood P A. 1999. Tectonothermal evolution of the Mayuan Assemblage in the Cathaysia Block; implications for Neoproterozoic collision-related assembly of the South China Craton. American Journal of Science, 299(4): 309–339, doi:

10.2475/ajs.299.4.309

Zhao Xilin, Mao Jianren, Ye Haimin, et al. 2013. New SHRIMP U-Pb zircon ages of granitic rocks in the Hida Belt, Japan: implications for tectonic correlation with Jiamushi massif. Island Arc, 22(4): 508–521, doi: 10.1111/iar.12045

Zhou Di, Chen Hanzong, Wu Shimin, et al. 2002. Opening of the South China Sea by dextral splitting of the East Asian continental margin. Acta Geologica Sinica (in Chinese), 76(2): 180–190

Zhou X M, Li Wuxian. 2000. Origin of Late Mesozoic igneous rocks in Southeastern China: implications for lithosphere subduction and underplating of mafic magmas. Tectonophysics, 326(3–4): 269–287

Zhou Xinmin, Sun Tao, Shen Weizhou, et al. 2006. Petrogenesis of Mesozoic granitoids and volcanic rocks in South China: a response to tectonic evolution. Episodes, 29(1): 26–33, doi: 10.18814/epiiugs/2006/v29i1/004

Zhu Weilin, Huang Baojia, Mi Lijun, et al. 2009. Geochemistry, origin, and deep-water exploration potential of natural gases in the Pearl River Mouth and Qiongdongnan basins, South China Sea. AAPG Bulletin, 93(6): 741–761, doi: 10.1306/02170908099

Zhu Weilin, Xie Xinong, Wang Zhenfeng, et al. 2017. New insights on the origin of the basement of the Xisha Uplift, South China Sea. Science China Earth Sciences, 60(12): 2214–2222, doi: 10.1007/s11430-017-9089-9

Supplementary information:

Table. S1. LA-ICPMS U-Pb zircon data for basement granitoids from the Qiongdongnan Basin.

Table. S2. Hf isotope composition of zircons for basement granitoids from the Qiongdongnan Basin.

Table. S3. Major and trace elements of the basement granitoids in the Qiongdongnan Basin.

The supplementary information is available online at https://doi.org/10.1007/s13131-022-2078-1 and http://www.aosocean.com/.

The supplementary information is published as submitted, without typesetting or editing. The responsibility for scientific accuracy and content remains entirely with the authors.